Nanometer-thin solid-state nanopores by cold ion beam sculpting

Aaron T. Kuan[1] and Jene A. Golovchenko[1,2]
[1]*School of Engineering and Applied Sciences, Harvard University, Cambridge, Massachusetts 02138, USA*
[2]*Department of Physics, Harvard University, Cambridge, Massachusetts 02138, USA*

(Received 20 April 2012; accepted 4 May 2012; published online 21 May 2012)

Recent work on protein nanopores indicates that single molecule characterization (including DNA sequencing) is possible when the length of the nanopore constriction is about a nanometer. Solid-state nanopores offer advantages in stability and tunability, but a scalable method for creating nanometer-thin solid-state pores has yet to be demonstrated. Here we demonstrate that solid-state nanopores with nanometer-thin constrictions can be produced by "cold ion beam sculpting," an original method that is broadly applicable to many materials, is easily scalable, and requires only modest instrumentation. © *2012 American Institute of Physics*. [http://dx.doi.org/10.1063/1.4719679]

Initially, "ion beam sculpting" was used to fabricate solid-state nanopores capable of detecting single DNA molecules.[1] That original process took advantage of the surprising observation that at room temperature a low energy argon ion beam can shrink large prefabricated pores in thin silicon nitride (SiN) and oxide membranes to single digit nanometer diameters, creating an accumulated volcano-like mound of material that defines the nanopore.[2] However, the material constituency and precise internal geometry (including thickness) of pores produced by this additive process are difficult to control and are not well characterized or understood. Ion beam sculpting has been semi-quantitatively described with an adatom diffusion model in which an ion beam induced electric field near the pore causes accumulation of mobile surface adatoms created by the ion beam.[3] The distance from the pore edge X_m within which adatoms are more likely to reach the pore than be annihilated by the ion beam or trapped at local surface defects is characterized by[4]

$$X_m = \left(\frac{1}{l_{trap}^2} + \frac{\sigma}{D}F\right)^{-\frac{1}{2}}, \tag{1}$$

where l_{trap} is the average distance between surface defects, σ is the cross section for adatom annihilation by an incident ion, D is the surface diffusivity of adatoms, and F is the ion flux.

At low temperatures, the surface diffusivity D can be reduced to the point that X_m approaches zero and prefabricated SiN pores open instead of close under ion beam exposure.[1,4] In this work we show that in the low temperature limit, surface diffusion is almost completely suppressed and removal of material by sputtering dominates pore formation, allowing the fabrication of very thin nanopores. This cold ion beam sculpting (CIBS) method does not require pre-existing pores and eliminates the "volcano phenomenon."

A focused ion beam (FIB) machine (FEI Micrion, 50 keV Ga) was used to mill a bowl-shaped (~100 nm diameter) cavity on one side of a ~250 nm thick free-standing silicon nitride (SiN) membrane. Then, in an ion sculpting apparatus described elsewhere[5] (Fig. 1(a)), the membrane was cooled below 173 K using liquid nitrogen and sputtered from the side opposite the cavity using a ~1 mm diameter pulsed ($\Delta T = 100$ ms) beam of 3 keV argon ions with flux $F = 1.65 \pm 0.28$ ions/(nm$^2 \cdot$ s). Ions transmitted through the membrane during sputtering were monitored using an electrostatic analyzer and a single ion detector (Channeltron). At first, no ions are observed because the membrane blocks the ion beam. As the membrane surface is sputtered away, it eventually breaks through the bottom of the bowl-shaped cavity on the opposite surface, creating a nanopore with a thin constriction (Fig. 1(b)). After breakthrough, the ions are transmitted with a count rate proportional to the area of the nanopore. This allows one to monitor the pore size in real-time and halt the process when the pore reaches a desired diameter.

To demonstrate this control we created pores of different diameters using the same argon ion flux F but varying the count rate at which the sputtering process was stopped. The diameter D of the pore is related to the instantaneous ion count rate at the end of the ion sculpting process $c(t_f)$ by

$$c(t_f) = \left(\frac{F\pi}{4}\right) D(t_f)^2. \tag{2}$$

However, the number of ions counted during the ith pulse C_i is the average of $c(t)$ over the pulse length ΔT. Using a third order Taylor approximation for $c(t)$, we can approximate $c(t_f)$ using C_i from the final three pulses, defining the adjusted final ion count $\tilde{C}_f$ as

$$\begin{aligned}\tilde{C}_f &\equiv c(t_f)\Delta T \\ &\approx C_f + \frac{1}{2}(C_f - C_{f-1}) + \frac{1}{3}(C_f - 2C_{f-1} + C_{f-2})\end{aligned} \tag{3}$$

and obtain an estimate of the pore diameter

$$D(t_f) \approx \frac{2}{\sqrt{\pi}}\sqrt{\frac{\tilde{C}_f}{F\Delta T}}. \tag{4}$$

In Fig. 2, the light blue band shows the expected relationship between adjusted ion counts and pore diameter given above; its width is determined by the systematic uncertainty in the ion flux. We also measured the diameters of the CIBS nanopores in a TEM (JEOL 2100) for each data point in Fig. 2.

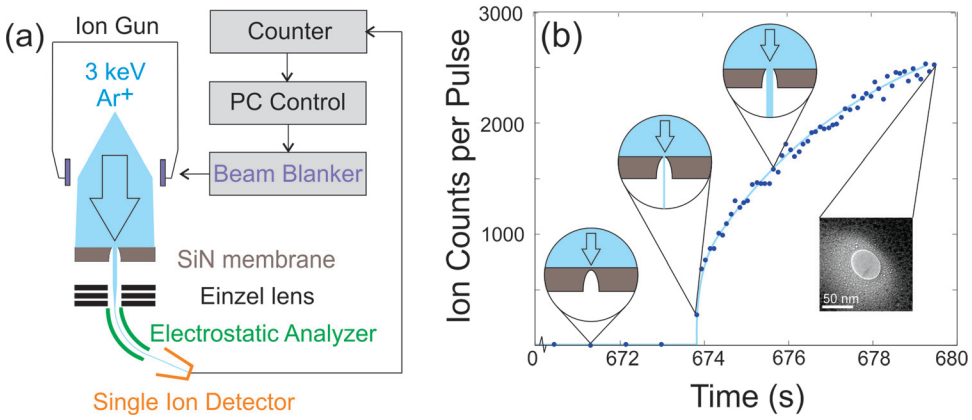

FIG. 1. Cold ion beam sculpting. (a) Schematic of ion sculpting system. (b) Count rate trace of cold ion beam sculpting of a 50 nm diameter nanopore in a SiN membrane. Data points indicate count rates for successive ion pulses. The line is merely a guide to the eye and is not a fit to the data. Inset: plan view TEM image of resulting nanopore.

The diameters and vertical error bars were determined from plan view TEM images (Fig. 2, insets) using a radial averaging algorithm,[6] and the horizontal error bars account for counting statistics. For pores $\geq$10 nm, the prediction of diameter based on $\tilde{C}_f$ is very accurate, but pores $<$10 nm appear larger than expected. This is most likely due to pore opening by electron sputtering during plan view TEM imaging. The accuracy of pore diameter control ultimately depends on the sputter yield, which determines how many ions one counts for a given amount of material removed. For argon ions on silicon nitride, pores as small as 6 nm in diameter could be fabricated reproducibly. Sputtering using ions with lower sputtering yields should allow even smaller pores to be fabricated.

Thickness profiles of solid-state nanopores have been previously estimated using energy filtered transmission electron microscopy (EFTEM) maps and electron tomography,[7,8] but these methods are not well suited for our study. EFTEM maps rely on a calculated mean free path, which is subject to error for materials that are not well-characterized, and tomography requires extensive electron exposure of the nanopore, which we have found to damage thin nanopores and modify their geometry.

Therefore, to characterize the profiles of the nanopore edges, we imaged cross-sections of the nanopores (along the plane of the membrane) using TEM. First, we coated the membrane on both sides with a 20 nm thick atomic layer deposition (ALD) of halfnium oxide (HfO_2)[9] that fills the nanopore conformally, creating a nanopore mold. This mold was then protected by depositing metal layers on both sides (100 nm Ag and 1 μm Pt on cavity and flat sides, respectively). Using a dual beam FIB-SEM system (Zeiss), we excised from the membrane a lamella ($\sim$2 μm thick) containing the filled nanopore, transferred the lamella to a TEM grid using a micro-manipulator (Omniprobe), and thinned it until it was electron transparent ($\sim$100 nm).[10] It is important to note that the pore is contained completely within the lamella—because the sample is imaged by transmission, the pore does not need to be cut in half by the FIB beam. Because of its higher atomic number, the HfO_2 gives strong scattering contrast compared to the SiN membrane. As a result, a projected cross-sectional image of the nanopore is produced (Figs. 3(a)–3(d), top). The resolution of this cross-sectional image is limited by the lamella thickness and varies from sample to sample. We determined the resolution empirically[11] by examining the edge between the HfO_2 layer and the SiN membrane away from the pore; for most samples the resolution was $\sim$1 nm.

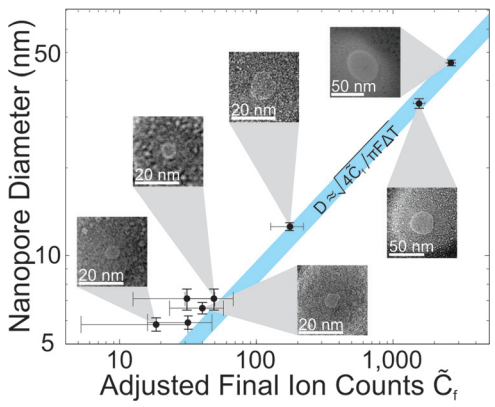

FIG. 2. Control of nanopore diameter using CIBS. Nanopore diameter as a function of adjusted final ion counts. The thick blue line indicates the expected pore diameters based on the ion flux; its width is due to uncertainty in the ion flux. Data markers represent diameters of CIBS nanopores fabricated in a SiN membrane as measured by TEM. Insets: TEM images of the nanopores from which the nanopore diameters were measured.

Since the pores have rounded edges, the most meaningful and important measure of the nanopore profile is the edge radius of curvature. The edge profiles of the pores were determined from the cross-sectional TEM images by following a constant intensity contour at the intensity value corresponding to the edge of the membrane, which was determined by inspecting a line profile across the interface between the SiN membrane and the HfO_2 layer. The edge radius was extracted from this contour (x_i, y_i) using a cubic least-squares fit $x_i - X_o = A(y_i - Y_0)^3 + B(y_i - Y_0)^2$, where the radius of curvature is $R = 1/2B$ (black curves in Figs. 3(a)–3(d), top). The uncertainty in R was propagated from the standard errors in the parameter B from the least-squares fit and the uncertainty in the intensity value defining the contour.

Fig. 3(a) shows a cross-sectional image of a CIBS nanopore with edge radius $R = 1.5 \pm 0.3$ nm. The incident argon ions sputtered the top side of the membrane where a $\sim$5 nm thick layer implanted with argon is visible. This depth is consistent with simulations performed using the ion stopping simulation (Stopping and Range of Ions in Matter (SRIM)).[12] The pore diameter $D = 6.6 \pm 0.3$ nm was measured from the

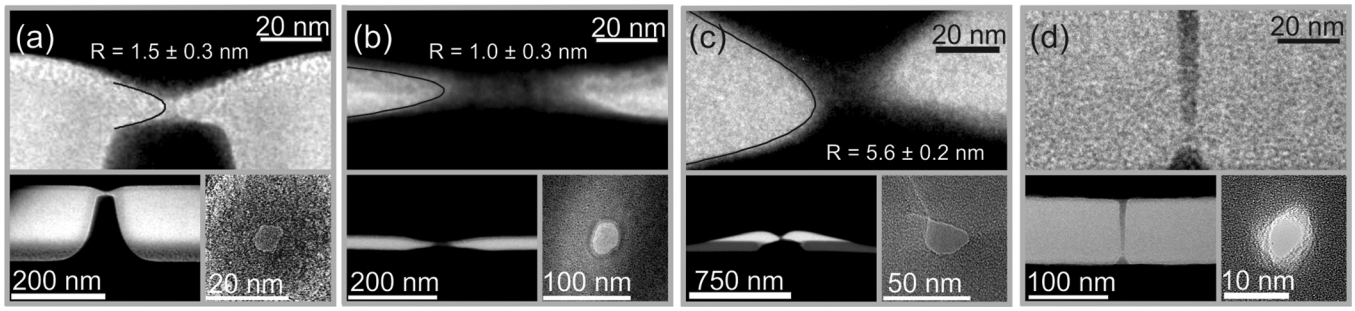

FIG. 3. Cross-sectional TEM images of CIBS and other nanopores. (a)-(d) Top: cross-sectional TEM images of nanopore edges with cubic polynomial fits of edge profiles (black curves). Bottom left: larger field of view cross-sectional TEM images. Bottom right: plan view TEM images of nanopores. (a) 6 nm diameter CIBS nanopore from a deep cavity. (b) 33 nm diameter CIBS nanopore from a shallow cavity. (c) 20 nm diameter room-temperature ion sculpted nanopore. (d) 6 nm diameter electron drilled nanopore.

plan view TEM image taken before the pore was filled with HfO_2 (Fig. 3(a), bottom right). A larger field-of-view cross-sectional image (Fig. 3(a), bottom left) reveals the shape of the cavity formed with the FIB on the bottom side of the membrane.

Very different pore profiles can be obtained from different cavity geometries, which depend on how deeply the cavities are milled into the SiN membrane. Fig. 3(b) shows a nanopore fabricated using a shallow cavity milled in an ~80 nm thick SiN membrane. The bottom of this cavity (Fig. 3(b), bottom left) is much flatter than the deep cavity shown in Fig. 3(a). The cross-sectional TEM image (Fig. 3(b), top) reveals a smaller edge radius ($R = 1.0 \pm 0.3$ nm) than the deep cavity CIBS pore. Away from the cavity, the SiN membrane has been thinned to ~30 nm. The pore diameter measured from the plan view image (Fig. 3(b), bottom right) $D = 33 \pm 3$ nm is consistent with the cross-sectional profile. Although the cavity geometry seems to have some effect on the edge radius, we hypothesize that the minimum edge radius for CIBS pores is ultimately limited by the ion penetration depth. This is because edges with radii much smaller than the ion range are quickly sputtered from the back and side surfaces. Therefore, even thinner edges may be obtained by using heavier ions or lower ion energies, both of which exhibit smaller penetration depths.

The top surface of the CIBS pores shown in Figs. 3(a) and 3(b) are observed to deflect downwards close to the pore. We attribute this effect to biaxial compressive stresses induced in the membrane by the FIB during cavity formation; its effects have been observed in free-standing silicon nitride films by Kim *et al.*[13] In preliminary experiments we have performed with cavities formed by reactive ion etching (RIE) rather than FIB, such deflections were not observed.

For comparison, we also imaged a silicon nitride nanopore fabricated by room temperature ion sculpting.[1] Fig. 3(c) demonstrates that it has a larger edge radius ($R = 5.6 \pm 0.2$ nm) than the CIBS pores. The large field-of-view cross-sectional image of the room temperature ion sculpted pore reveals the volcano-like mound of accumulated adatom material (Fig. 3(c), bottom left), which is significantly less dense than and probably quite different from the original membrane material. Future work will focus on identifying the nature of this material.

An electron beam drilled nanopore[14] was also imaged (Fig. 3(d)), revealing that the pore has an asymmetric hourglass shape. Since the walls of the pore are almost straight, the thickness of the pore is approximately the thickness of the membrane (~80 nm). One can produce thinner pores with the electron beam drilling method by starting with thinner membranes: Wanunu *et al.* have demonstrated that SiN membranes as thin as 6 nm are robust enough to support electron beam drilled nanopore devices.[15]

To demonstrate the feasibility of CIBS nanopores as single molecule sensors, we measured the noise power spectral densities (PSD) (Fig. 4(a)), and translocations of 10 kbp dsDNA (New England Biolabs) (Fig. 4(b)) through an

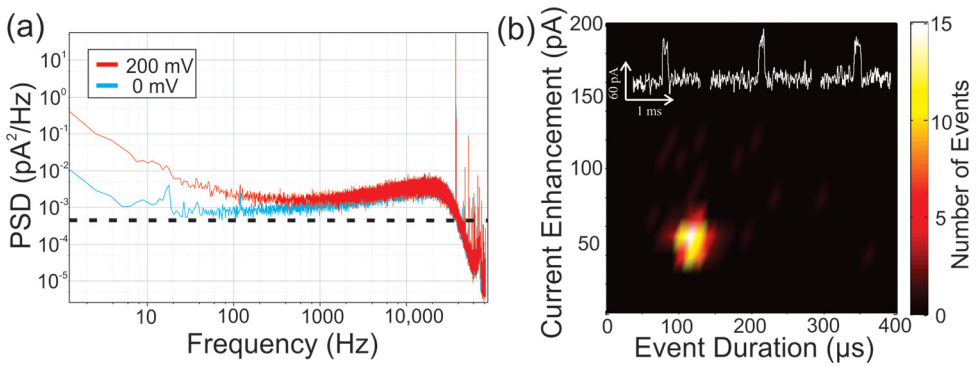

FIG. 4. DNA translocations through an 8 nm CIBS pore. (a) Noise power spectral density of current through nanopore with no bias (cyan) and with 200 mV bias (red) in 100 mM KCl, *p*H 10. The dashed line indicates expected thermal noise. (b) Histogram of 108 DNA translocation events with a 200 mV bias (10 kbp dsDNA in 100 mM KCl solution), showing clustering around 57 pA, 132 μs events. White traces: 3 typical current-time traces of translocation events.

~8 nm diameter nanopore similar to that shown in Fig. 3(a). Nanopores were characterized in a 100 mM KCl/10 mM Tris/1 mM EDTA solution at *p*H 10 using a custom flowcell with Ag/AgCl electrodes and a patch clamp amplifier (Axopatch) filtered through a 20 kHz low pass filter. The pore exhibited a zero-bias conductance $G = 27.9 \pm 0.5$ nS. At low frequencies (<100 Hz), the power spectral density is dominated by $1/f$ noise, whereas at higher frequencies only thermal (Fig. 4(a), dashed line) and capacitively coupled preamplifier noise are observed.[16,17] At 100 mM salt, DNA translocation can be detected by ionic current enhancements due to the counter ions around the DNA molecule acting as mobile charge carriers.[18] Here we detected gel-purified 10 kbp fragments of λ dsDNA (New England Biolabs, ~12.5 μg/mL) with a 200 mV bias (Fig. 4(b)), observing predominantly unfolded events (white traces). The histogram of the current enhancement versus event duration shows clustering around events with median current enhancements of 57 pA and median duration of 132 μs.

The experiments described in this letter demonstrate that nanopores with edge radii as small as 1 nm and diameters as small as 6 nm can be reliably fabricated using CIBS. Practical upscaling of the CIBS process can be achieved using wafer-scale lithography methods (photolithography and RIE) to prepare the cavities and a broad ion beam to create the pores. Moreover, we believe that even smaller and thinner pores can be obtained with CIBS using lower energies and/or different sputter ions. Due to their very small effective thickness (comparable to single and multilayer graphene nanopores[19–21]) and scalable fabrication, CIBS nanopores are ideal candidates for solid-state nanopore DNA sequencing systems.

A.K. acknowledges T. S. Kuan for advice regarding TEM sample preparation, D. P. Hoogerheide for advice regarding data analysis, F. Albertorio and E. Brandin for assistance and advice regarding DNA translocation experiments, D. Vlassarev for assistance analyzing DNA translocation data, and C. J. Russo and R. Aubut for technical assistance with the ion sculpting system. Sample preparation and microscopy were performed at the Harvard Center for Nanoscale Systems in Cambridge, MA. This work was supported by National Institutes of Health Award R01HG003703 to J. A. Golovchenko.

[1]J. Li, D. Stein, C. McMullan, D. Branton, M. J. Aziz, and J. A. Golovchenko, Nature (London) **412**, 166 (2001).
[2]T. Mitsui, D. Stein, Y.-R. Kim, D. Hoogerheide, and J. Golovchenko, Phys. Rev. Lett. **96**, 036102 (2006).
[3]Q. Cai, B. Ledden, E. Krueger, J. A. Golovchenko, and J. Li, J. Appl. Phys. **100**, 024914 (2006).
[4]D. P. Hoogerheide, H. B. George, J. A. Golovchenko, and M. J. Aziz, J. Appl. Phys. **109**, 074312 (2011).
[5]D. M. Stein, C. J. McMullan, J. Li, and J. A. Golovchenko, Rev. Sci. Instrum. **75**, 900 (2004).
[6]C. J. Russo and J. A. Golovchenko, Proc. Natl. Acad. Sci. U.S.A. **109**, 5953 (2012).
[7]M.-Y. Wu, R. M. M. Smeets, M. Zandbergen, U. Ziese, D. Krapf, P. E. Batson, N. H. Dekker, C. Dekker, and H. W. Zandbergen, Nano Lett. **9**, 479 (2008).
[8]M. J. Kim, M. Wanunu, D. C. Bell, and A. Meller, Adv. Mater. **18**, 3149 (2006).
[9]D. M. Hausmann, E. Kim, J. Becker, and R. G. Gordon, Chem. Mater. **14**, 4350 (2002).
[10]U. Muehle, S. Jansen, L. Hillmann, H.-J. Engelmann, and D. Rafaja, in *Microscopy: Science, Technology, Applications and Education*, edited by A. Mendez-Vilas and J. Diaz (Formatex, 2012), pp. 1704–1716.
[11]L. Reimer and P. Gentsch, Ultramicroscopy **1**, 1 (1974).
[12]J. F. Ziegler, M. D. Ziegler, and J. P. Biersack, Nucl. Instrum. Methods Phys. Res. B **268**, 1818 (2010).
[13]Y. R. Kim, P. Chen, M. J. Aziz, D. Branton, and J. J. Vlassak, J. Appl. Phys. **100**, 104322 (2006).
[14]A. J. Storm, J. H. Chen, X. S. Ling, H. W. Zandbergen, and C. Dekker, Nat. Mater. **2**, 537 (2003).
[15]M. Wanunu, T. Dadosh, V. Ray, J. Jin, L. McReynolds, and M. Drndić, Nat. Nano **5**, 807 (2010).
[16]D. P. Hoogerheide, S. Garaj, and J. A. Golovchenko, Phys. Rev. Lett. **102**, 256804 (2009).
[17]R. M. M. Smeets, U. F. Keyser, N. H. Dekker, and C. Dekker, Proc. Natl. Acad. U.S.A. **105**, 417 (2008).
[18]R. M. M. Smeets, U. F. Keyser, D. Krapf, M.-Y. Wu, N. H. Dekker, and C. Dekker, Nano Lett. **6**, 89 (2006).
[19]S. Garaj, W. Hubbard, A. Reina, J. Kong, D. Branton, and J. A. Golovchenko, Nature (London) **467**, 190 (2010).
[20]G. F. Schneider, S. W. Kowalczyk, V. E. Calado, G. Pandraud, H. W. Zandbergen, L. M. K. Vandersypen, and C. Dekker, Nano Lett. **10**, 3163 (2010).
[21]C. A. Merchant, K. Healy, M. Wanunu, V. Ray, N. Peterman, J. Bartel, M. D. Fischbein, K. Venta, Z. Luo, A. T. C. Johnson, and M. Drndić, Nano Lett. **10**, 2915 (2010).